astro-ph/9508028

Triggering of Imaging Air Cherenkov Telescopes: PMT trigger rates due to night-sky photons

G. Hermann, C. Köhler, T. Kutter, W. Hofmann

Max-Planck-Institut für Kernphysik, P.O.Box 103980, 69029 Heidelberg, Germany

February 1, 2008

Abstract

Imaging air Cherenkov telescopes are usually triggered on a coincidence of two or sometimes more pixels, with discriminator thresholds in excess of 20 photoelectrons applied for each pixel. These thresholds required to suppress night-sky background are significantly higher than expected on the basis of a Poisson distribution in the number of night-sky photoelectrons generated during the characteristic signal integration time. We studied noise trigger rates under controlled conditions using an artificial background light source. Large tails in the PMT amplitude response to single photoelectrons are identified as a dominant contribution to noise triggers. The rate of such events is very sensitive to PMT operating parameters.

1 Introduction

Imaging Air Cherenkov Telescopes (IACTs) [1] have evolved into one of the most important tools for ground-based γ-ray astronomy in the TeV energy range. In an IACT, Cherenkov light emitted by particles of an extended air shower is imaged by a large mirror onto a camera consisting of an array of photomultiplier tubes (PMTs). Mirror sizes range from a few to almost 100 m^2; initially, cameras consisted of some tens of phototubes ("pixels"), whereas the latest generation of cameras now in operation or under construction frequently has several hundred phototubes, resulting both in an enhanced resolution of the image and in an improved field of view. The orientation and shape of the Cherenkov image are related to the direction and type of the primary particle, and can be used to separate γ-rays from the otherwise overwhelming background of charged cosmic rays. The total light yield in the image provides a measure for the energy of the primary.

To initiate the digitization of the signals from the camera, and of the read out of data, a trigger signal is required. Usually, this trigger signal is derived from the camera itself. In order to suppress spurious signals, two or more camera pixels have to fire in coincidence, with pulse heights exceeding a threshold $q_\circ$. The threshold value is usually quoted in units of the mean pulse height per photoelectron. The dominant source of spurious triggers are photons of the night-sky background (NSB) light, with a flux of about $2 \cdot 10^{12}$ photons/m^2 sr s in the relevant spectral range from 300 to 600 nm [2, 3, 4, 5]. For a telescope with 5 m^2 mirror area and an effective pixel diameter of 0.4° this translates into a photoelectron rate of about 30 MHz per pixel. In order to prevent random coincidences between pixels from saturating the data acquisition system, rather high trigger thresholds for the individual PMTs have to be chosen. Typical telescopes [6, 7] with a two-fold trigger coincidence require trigger thresholds of 20 or more photoelectrons in each PMT. As we shall see, these threshold values are generally much higher than expected based on the Poisson fluctuation in the number of NSB photoelectrons.

Topic of this paper is the study and interpretation of the single-PMT trigger rates and the optimization of the behaviour of the individual PMTs of a camera. We will first briefly review the expected night-sky trigger rates. We then describe the experimental setup used to study the trigger rates of PMTs and present the experimental results and their interpretation.

This work was carried out in preparation of the construction of the HEGRA IACT system - an array of 5 Cherenkov telescopes now under deployment at the Canarian island of La Palma. These telescopes will have about 8.3 m^2 mirror area, 5 m focal length, and will be equipped with cameras consisting of up to 271 PMT pixels with size corresponding to 0.25°. It is planned to use Thorn-EMI 9083 PMTs, equipped with a short light funnel with a hexagonal entrance area. An additional prototype telescope has a mirror area of 5 m^2, and an initial camera consisting of 37 Russian FEU-130 PMTs, each subtending a field of view of 0.4°. A detailed description of this telescope − whose camera is meanwhile upgraded to 127 Thorn-EMI pixels − is found in [7].

2 Expected single-PMT trigger rates and coincidence rates

In the following we review estimates for the rates at which individual pixels and the trigger coincidence fire.

Let us assume, for simplicity, that the individual pixels of a camera fire at identical rates R_{pixel}, and that all discriminator output pulses have the same length T. If the coincidence unit reacts instantaneously, the rate R_n of random n-pixel coincidences is approximately (for $R_{pixel}T \ll 1$):

$$R_n = nC_nR_{pixel}\,(R_{pixel}T)^{n-1} \quad . \tag{1}$$

The coefficient C_n gives the number of different n-pixel combinations; for a two-fold coincidence of M pixels, $C_n = M(M-1)/2$. Typical coincidence windows T range from 10 to 20 ns; acceptable IACT trigger rates R_n are usually in the range of a few Hz. For a two-fold coincidence of the 37 pixels of the HEGRA prototype telescope, e.g., these numbers imply single-pixel trigger rates of a few 100 Hz, many orders of magnitude below the 30-MHz rate at which single photoelectrons are generated by NSB. Obviously, trigger thresholds have to be chosen high enough such that only rare fluctuations trigger a pixel.

To estimate the single-pixel rates R_{pixel} for a given discriminator threshold, a usual approach is the following: the single-photoelectron pulse response of the PMT is approximated as a rectangle of length τ, the characteristic

shaping time. A discriminator with its threshold set at $q_\circ$ photoelectrons will then trigger if within a time τ at least $q_\circ$ photoelectrons are generated. Assuming that the individual night sky photons, and hence the photoelectrons are uncorrelated, the rate $R_{pixel}(q_\circ)$ can be estimated to

$$R_{pixel}(q_\circ) \approx R_{pe} \frac{(R_{pe}\tau)^{q_\circ - 1}}{(q_\circ - 1)!} e^{-R_{pe}\tau} \tag{2}$$

where R_{pe} is the rate at which photoelectrons are generated, provided that the rate is small, $R_{pixel} \ll R_{pe}$.

In order to reduce random IACT triggers, two factors appear to be rele-vant: a short coincidence resolution time T is useful (but in case of the usual 2-fold coincidence not too crucial, given that the rate R_2 depends only linearly on T). More important is a fast response τ of the PMT, ideally close to the spread of a few ns of the genuine Cherenkov photons; for the required large thresholds $q_\circ \gg 1$ this shaping time enters with a high power.

A short estimate shows that based on these equations, a threshold of about 7 photoelectrons should reduce the random trigger rate of a single PMT of the HEGRA-CT1 to well below 300 Hz, and hence the random coincidence rate R_2 to below one Hz. Operational experience, on the other hand, shows that much larger trigger thresholds are required, indicating that there are additional sources of PMT pulse-height fluctuations.

The rate estimates given above neglect a number of effects. For example, the pulse-height discriminator is often AC-coupled to the PMT. The threshold is hence applied relative to the time-averaged amplitude, resulting in a small shift. Also, the output pulse from the PMT is not rectangular. However, it is easy to see that approximating the pulse by a rectangular pulse of the same peak height and fwhm, pile-up is overestimated rather than underestimated. Finally, the single-photoelectron pulse spectrum generated by a PMT is usually not a narrow line, but instead a rather broad spectrum of relative width $w \approx 0.5 - 1$. Hence, the rms noise is increased by a factor $\sqrt{1 + w^2} \approx 1.1 - 1.5$; the required threshold $q_\circ$ should increase by a similar factor. None of these factors explains the discrepancy between estimated and actually required thresholds.

Electronics noise could be another source of random triggers, but rate measurements with a closed camera lid usually identify night-sky photons as the dominant source of random triggers.

To provide more insight into the statistics of the amplification process, we calculated the expected distribution of pulse heights at the output of the PMT and the trigger rates based on the assumption that at each dynode the number of secondary electrons generated by a primary electron follows a Poisson distribution. Lacking an exact analytical expression, the response was calculated by numerically convoluting the distributions for the various stages of dynode amplification. To describe the response of the PMT in terms of an equivalent number of photoelectrons at its input, the resulting pulse heights were rescaled to the mean pulse height for a single photoelectron, corresponding to a total gain $G = \Pi g_n$, where g_n is the gain of the n^{th} dynode. We used $g_1 = 5$ and $g_n = 2.5$ for $n > 1$, corresponding roughly to the mean gain of BeCu dynodes at the typical voltages applied in our tests [8]. Fig. 5 shows the resulting distribution of pulse heights for a single photoelectron. Fig. 5 illustrates the modeled trigger rate as a function of the NSB photoelectron yield. The modeled PMT trigger rate shows two distinct regimes:

- For a very small mean number of photoelectrons per integration interval τ, the trigger probability is directly proportional to the NSB photoelectron rate. In this regime, upward fluctuations of the single-photoelectron response cause triggers. The rate is much higher than expected on the basis of fluctuations in the number of photoelectrons per integration interval, and is quite insensitive to the pulse length τ.
- For higher photoelectron rates the trigger probability grows with a higher power of the NSB photoelectron rate. In this regime, pile-up of photoelectrons causes triggers. The trigger rate rises steeply with the pulse length τ.

3 Experimental setup and measurement procedure

Rather than using actual night-sky light, the experimental trigger studies were carried out with an artificial source of background light, in order to generate reproducible conditions. For all practical purposes, only the rate at which "night sky" photoelectrons are generated should matter, and not details of the spectrum of the incident light.

In our setup, the PMT under test (usually a Thorn-EMI 9083) is illuminated by a dim DC light source; we use either a small filament lamp or a LED. In order to study the time structure of PMT pulses, a pulsed fast LED as well as a laser with about 1 ns pulse length is available. The PMT output is coupled to a fast amplifier (LeCroy 612 AM), which is connected via 15 m of RG178 cable to a fan-out. A similar setup will be used in the real telescopes, where a preamplifier is mounted in the camera, and the ADCs and discriminators are located in crates near the telescope. Despite its bandwidth limitations, RG178 cable is used in order to limit the cross section and the weight of the cable bundles. At the end of the cable, the PMT signal has a typical width of about 5 ns (fwhm). One output of the fan-out is routed to a discriminator (LeCroy 821), the other, via a delay, to a charge-sensitive ADC (LeCroy 2249A) gated by the discriminator signal. Alternatively, a Flash-ADC system is used to record the pulse shapes, in particular to search for afterpulses. Discriminator trigger rates are measured with a scaler. The PMT current is monitored by switching the PMT output to an electrometer. During a sequence of measurements, either the discriminator threshold or the light intensity is varied. To investigate the influence of the signal shaping time, shaping amplifiers (Canberra 2111) could be added, resulting in pulse lengths of 15 ns or 30 ns fwhm.

Two critical constants have to be determined in order to calibrate the system: the relation between the discriminator threshold voltage and the equivalent number of photoelectrons, and the relation between the PMT DC current and the (otherwise uncalibrated) photon flux. We use the single-photoelectron peak to determine these coefficients. The charge spectrum measured at low light levels and with a low threshold setting is shown in Fig. 5(a), already corrected for the ADC pedestal and after subtraction of the dark-count spectrum accumulated over the same time [1]. With a higher discriminator threshold setting, a relatively sharp cutoff in the spectrum is seen. Adjusting the threshold until the cutoff is at the position of the

[1]We note that the spectrum shows a feature not reproduced in the simulation: an excess at low pulse heights, which fills up the region below the peak and which generates a peaking near zero charge. The origin of these events is quasielastic backscattering of the photoelectron from the first dynode, without multiplication [9]. It can also happen that the photoelectron misses the first dynode entirely, and lands directly on the second dynode. In either case, the overall gain is reduced by the gain of the first dynode, and because of the smaller gain of the second dynode, the peak is smeared out.

single-photoelectron peak allows a rather precise calibration of the threshold in units of photoelectrons, after correction for offsets and pedestals. At lower operating voltages, the single-photoelectron peak is not always well enough separated to use this technique. In such cases, the calibration factor is determined at a higher voltage and then scaled down in proportion to the PMT gain as derived from the ratio of the DC currents at the two voltages, measured at the same light flux. For an asymmetric single-photoelectron peak such as the one seen in Fig. 5, a principal question is whether the calibration should refer to the peak position, i.e., the *most probable* pulse height, or to the *average* pulse height. We use the peak position as the easier and more reliable measurement. We estimate the systematic difference between the most probable and the average pulse height to be less than 10 to 15 %.

The single-photoelectron rate R_{pe} for a given light intensity can be obtained either by directly counting events with a low threshold, or based on the PMT average current I and the (average) charge gain G of the PMT,

$$R_{pe} = \frac{I}{Ge} \quad , \tag{3}$$

with the elementary charge e. We determine the charge gain using the position of the single-photoelectron peak in the ADC spectrum. With either method to measure R_{pe}, the behavior of the spectrum at very low pulse heights causes systematic uncertainties. The agreement between the two methods to determine the photoelectron rate − counting or current measurement − depended somewhat on the particular PMT used. Typically, the values agreed within 10 to 15%.

In summary, we estimate that scale uncertainties in the calibration of the discriminator threshold in units of photoelectrons amount to 15 %, and that the photoelectron rate has a similar systematic uncertainty.

4 PMT trigger rates

Fig. 5 shows a typical set of measurements carried out using an Thorn-EMI 9083 PMT. Operated as 10-dynode PMT, the tube provides too much gain for use in an IACT, resulting in large anode currents for typical NSB levels. Therefore, the signals were derived from the 9th dynode, with the 10th dynode and the anode connected to the same potential. We used a resistive voltage divider, with resistor ratios 2:1.5:1:1... (starting from the photo cathode). The divider was optimized to provide maximum homogeneity and size of the active surface, and good linearity.

In Fig. 5 we illustrate how the PMT trigger rates depend on various parameters, such as the trigger threshold $q_\circ$ (a), the light level (expressed in terms of the photoelectron rate) (b), the pulse length (c) and the high voltage applied to the PMT, with the trigger threshold kept constant in units of photoelectrons (d). Statistical errors on the data points are generally negligible, except for low rates in the Hz region; even there, statistical errors are generally below 10%. Complete sets of measurements were repeated after several days, including the determination of calibration constants, and showed that rates are reproduced within 15%. For a given PMT current, illumination with a filament lamp and a LED results in identical trigger rates, within 5%. Different PMTs of the same type (and from the same production batch) showed similar trigger rates, within a factor of 2.

The results shown in Fig. 5 (a),(b),(c) agree qualitatively with our expectations; trigger rates drop with increasing threshold, with decreasing light level, and with decreasing shaping time. Quantitatively, they are however in striking contrast with the model calculations (Fig. 5):

- With increasing threshold, trigger rates fall much more slowly than expected on the basis of a Poisson distribution in the number of photoelectrons, even including the gain fluctuations.
- The absolute trigger rates for large thresholds are several orders of magnitude larger than expected.
- The trigger rate depends linearly on the light yield over almost the entire range of light levels. Only for the highest levels the dependence steepens.

- The influence of the pulse length is relatively modest; based on eq. 2 a change from 5 ns pulse length to 30 ns at a threshold $q_\circ = 15$ should increase the rate by about 8 orders of magnitude, compared to an observed increase of less than 10.

- Finally, as the single-photoelectron peak narrows with increasing high voltage, one would expect the rate to decrease slightly, when the voltage is increased, and the threshold is adjusted to correspond to a fixed number of photoelectrons. In contrast, the data show a significant increase of the rate with the PMT operating voltage. For $q_\circ = 15$, e. g., the trigger rate rises with the 1.8^{th} power of the PMT gain.

The obvious interpretation of these observations is that gain fluctuations have a much larger tail towards large pulse heights than expected; these gain fluctuations dominate over the Poisson fluctuations in the number of photoelectrons over nearly the entire range in R_{pe}. The presence of such a tail in the PMT response is indeed evident from the charge spectrum of single-photoelectron signals, once it is plotted on a logarihmic scale (Fig. 5 (b)). At levels below about $3 \cdot 10^{-3}$ of the peak, a long and flat tail takes over from the steep descent of charge spectra right beyond the peak. In the region of IACT trigger thresholds, this tail dominates. The tail is not caused by background events unrelated to the illumination; the fraction of events in the tail is constant over a wide range of light levels. The observation of this tail is not limited to the Thorn-EMI 9083 PMT; similar behaviour was observed for the Philips XP2020, and for the (in its construction completely different) Hamamatsu R5600P, although the relative level of the tail differed.

5 Origin of the amplitude tail and optimization of PMT trigger properties

In order to identify the origin of the large pulses, which cause the high trigger rates, we considered first the high-voltage dependence of the phenomenon. The voltage of the early stages (photocathode to 4th dynode) and of the later stages were varied independently (see Fig. 5). The level of the tail is sensitive to the field strenght in the early stages, and quite insensitive to the later stages. As a candidate mechanism to generate the large pulses, the

ionization of rest gas on or near the first dynode emerged. Studies with the fast LED as a pulsed light source and the Flash-ADC system to record the time history of the signals did indeed reveal afterpulses following about 500 ns after the light pulse (Fig. 5). This delay is consistent with the propagation time [10] of an ion back to the photocathode, where its impact releases a large number of electrons, which are then subsequently amplified and generate a large output pulse. Varying the voltage V applied to the PMT, the delay ΔT was observed to vary as expected for such a mechanism, $\Delta T \propto 1/\sqrt{V}$. Using the pulsed light source, we could separately record the pulse height distributions of both prompt and delayed pulses. Fig. 5 illustrates that indeed for prompt pulses (first 20 ns after the LED pulse) the large-amplitude tail is significantly reduced, whereas the delayed pulses (around 450 to 550 ns) include the large-pulseheight tail causing most of the triggers for large $q_\circ$.

What do these observations imply for the optimization of IACT trigger schemes? Given the high photoelectron rate, an active veto of delayed pulses seems excluded, since it would generate enormous dead time. Since a major source of rest gas in PMTs is the diffusion of Helium in the atmosphere through the PMT walls [10], an effective reduction of the rest gas pressure appears difficult. A relatively simple means, however, is the reduction of the voltage applied to the PMT; a lower field in the space between photo cathode and 1st dynode reduces both the probability for ionization, and the reacceleration of ions. Usually, PMT voltages are optimized for optimal electron collection and a good single-photoelectron peak. Given that at least some telescopes operate with conversion factors of about 1 ADC channel per photoelectron, a slightly-wider than optimal single-photoelectron peak seems tolerable. We conclude that the voltage between photocathode and 1st dynode should be chosen near the minimum required for homogenous electron collection and response.

Acknowledgements

We thank T. Lohse for contributions to the numerical modeling of the PMT trigger rates. We acknowledge discussions with members of the HEGRA-IACT group, in particular with R. Mirzoyan. After completion of this work, we learned that he arrived at similar conclusions concerning IACT trigger rates.

References

[1] T.C. Weekes, Space Sci. Rev. 59 (1992) 315

[2] F.E. Roach and J.L. Gordon, The Light of the Night Sky, D. Reidel Publishing Company, Dordrecht, Holland (1973)

[3] A. Akhperjanian and C. Wiedner, HEGRA Internal Note (1993)

[4] R. Mirzoyan and E. Lorenz, MPI-PhE/95-35 (1994)

[5] C.R. Jenkins and W.S. Unger, The Night Sky Spectrum at La Palma, ING Technical Note # 82, Royal Greenwhich Observatory, Cambridge

[6] M.F. Cawley et al., Exp. Astronomy 1 (1990) 173

[7] R. Mirzoyan et al., Nucl. Instr. Meth. A351 (1994) 513

[8] Photomultiplier and accessory catalog, Thorn EMI Electron Tubes Limited (1993)

[9] Photomultiplier tubes - principles & applications, Section 2.1, Philips, (1994)

[10] Dito, Section 5.7

Figure captions

Figure 1. Distribution of PMT output pulse heights, scaled to the mean output for one photoelectron, modeled assuming a Poisson distribution in the number of secondary electrons, with gain 5 for the first dynode, and gain 2.5 for the others. The Distribution is shown with logarithmic and linear (small picture) scale for the relative number of events.

Figure 2. Modeled PMT trigger rate as a function of the NSB photoelectron yield, for 5 ns and 30 ns PMT output pulse width, and for a trigger treshold $q_\circ = 5$. The curves illustrate separately the effects of poissonean fluctuations in the arrival of photoelectrons (a), as estimated by eq. 2, and of fluctuations in the amplification of single photoelectrons (b), as well as the full numerical calculation including both effects (c).

Figure 3. (a) Typical measured single-photoelectron spectrum of an Thorn-EMI 9083 PMT, after subtraction of the dark-count rate. The PMT is illuminated with DC light, and the readout is triggered by the PMT signal.
(b) Same, but with logarithmic scale.

Figure 4. Trigger rates measured using a Thorn-EMI 9083 PMT, with the signal derived from the 9th dynode. The nominal operating voltage was 887 V. (a) Trigger rate as a function of the discriminator threshold $q_\circ$, for different light levels (expressed in terms of the photoelectron rate). (b) Trigger rate as function of light level, for different discriminator thresholds $q_\circ$.
(c) Trigger rate as a function of the discriminator threshold, for different shaping time constants, resulting in 5, 15, and 30 ns pulse length (fwhm).
(d) Trigger rate as a function of the high voltage applied to the PMT, with discriminator threshold adjusted to correspond to a fixed number of photoelectrons, $q_\circ = 10$ and $q_\circ = 15$.

Figure 5. Charge spectrum obtained for low-level (single-photoelectron) illumination of the PMT, with a resistive voltage divider 2R-1.5R-1R-1R-1R... (starting from the photocathode). (a) For two different voltage levels in the early part of the chain, up to dynode 4, and (b) for two different voltage

levels in the late part, dynodes 4 to 9. The voltage levels given refer to the voltage across a resistor 1R, in the early and the late part of the dynode chain.

Figure 6. Arrival time t of charge pulses from the PMT, following the illumination with a light pulse at the single-photoelecton level at $t \approx 0$. The output of the PMT was recorded by a Flash-ADC system. The prompt pulses near $t \approx 0$ are suppressed.

Figure 7. Charge spectrum of "prompt" (20 ns window after the LED flash) and "delayed" (450-550 ns after the LED flash) PMT pulses, for single-photoelectron illumination with a pulsed LED. The solid line represents the spectrum obtained if no correlation to the LED flash is requested.

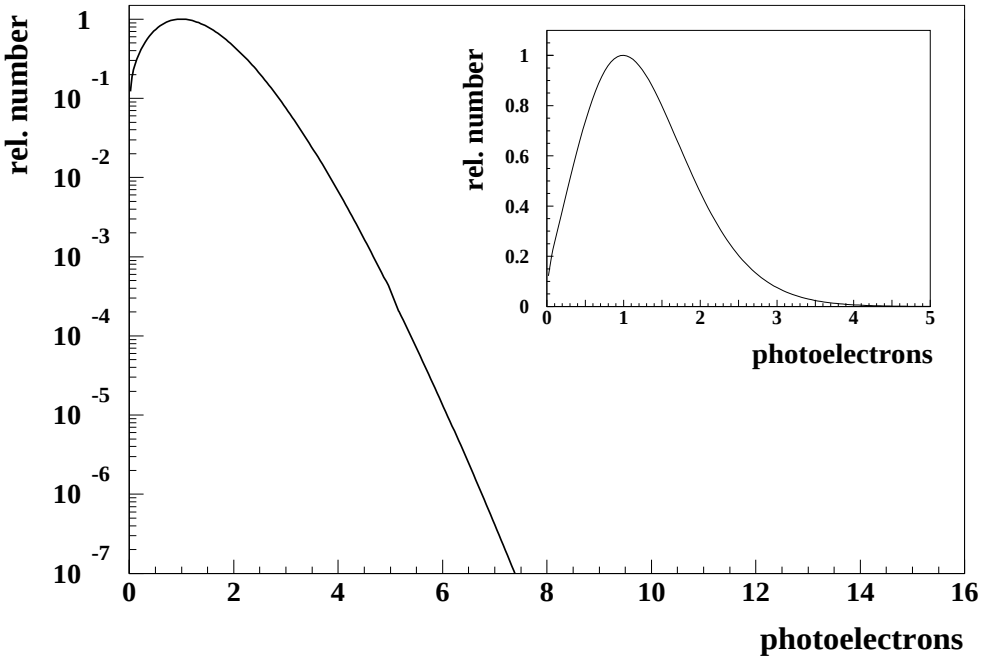
rel. number
1
10^-1
10^-2
10^-3
10^-4
10^-5
10^-6
10^-7
0
2
4
6
8
10
12
14
16
photoelectrons
rel. number
1
0.8
0.6
0.4
0.2
0
0
1
2
3
4
5
photoelectrons

Figure 1:

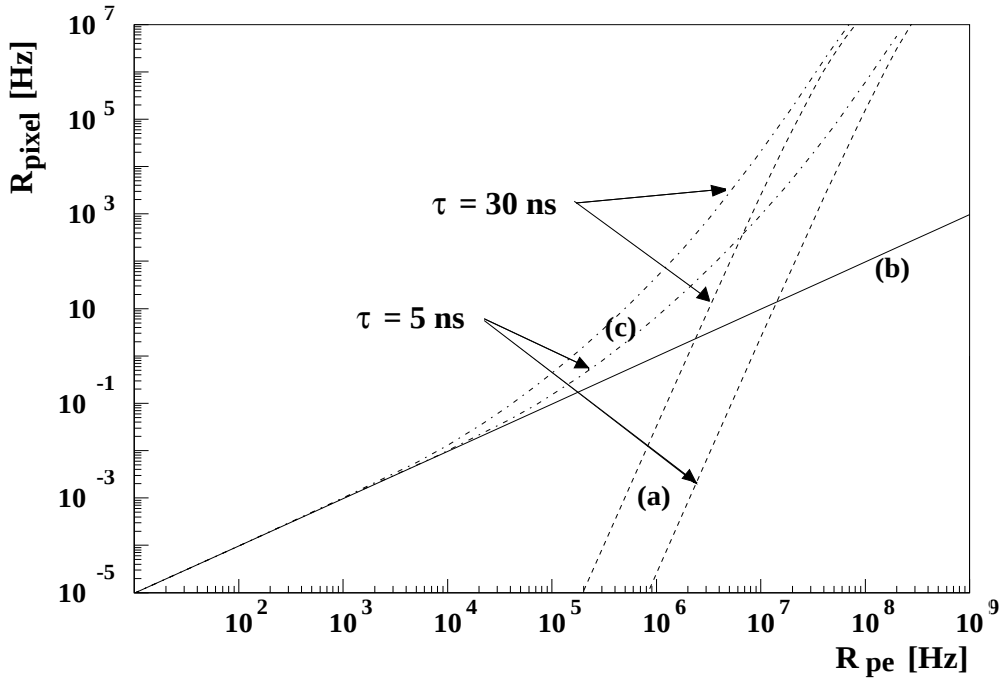
R_{pixel} [Hz]
10^{7}
10^{5}
10^{3}
10
10^{-1}
10^{-3}
10^{-5}
10^{2}
10^{3}
10^{4}
10^{5}
10^{6}
10^{7}
10^{8}
10^{9}
R_{pe} [Hz]
τ = 30 ns
τ = 5 ns
(a)
(b)
(c)

Figure 2:

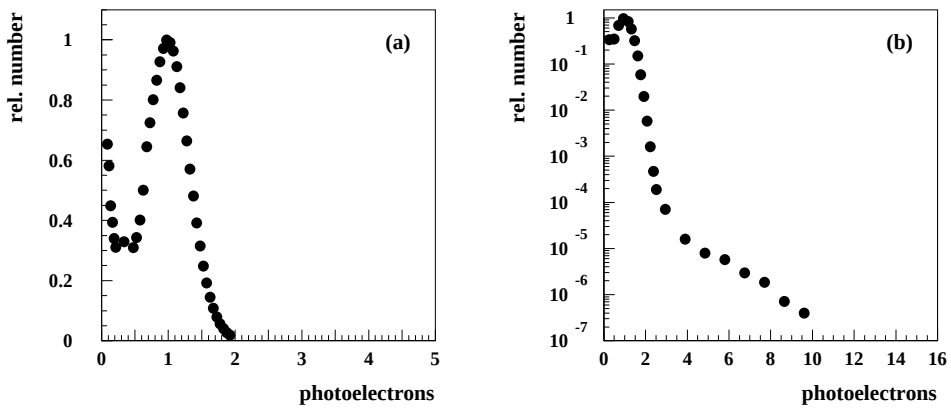

Figure 3: a,b

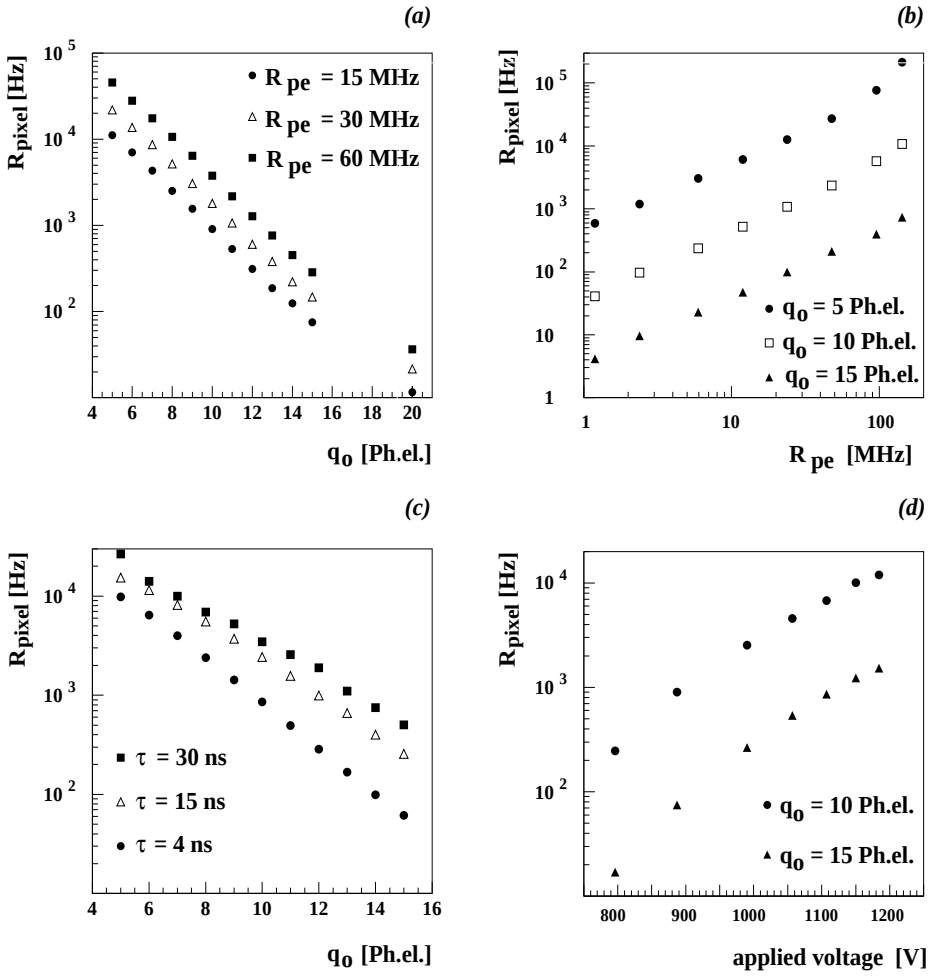
(a)
R pixel [Hz]
R pe = 15 MHz
R pe = 30 MHz
R pe = 60 MHz
q0 [Ph.el.]
(b)
R pixel [Hz]
q0 = 5 Ph.el.
q0 = 10 Ph.el.
q0 = 15 Ph.el.
R pe [MHz]
(c)
R pixel [Hz]
τ = 30 ns
τ = 15 ns
τ = 4 ns
q0 [Ph.el.]
(d)
R pixel [Hz]
q0 = 10 Ph.el.
q0 = 15 Ph.el.
applied voltage [V]

Figure 4: a-d

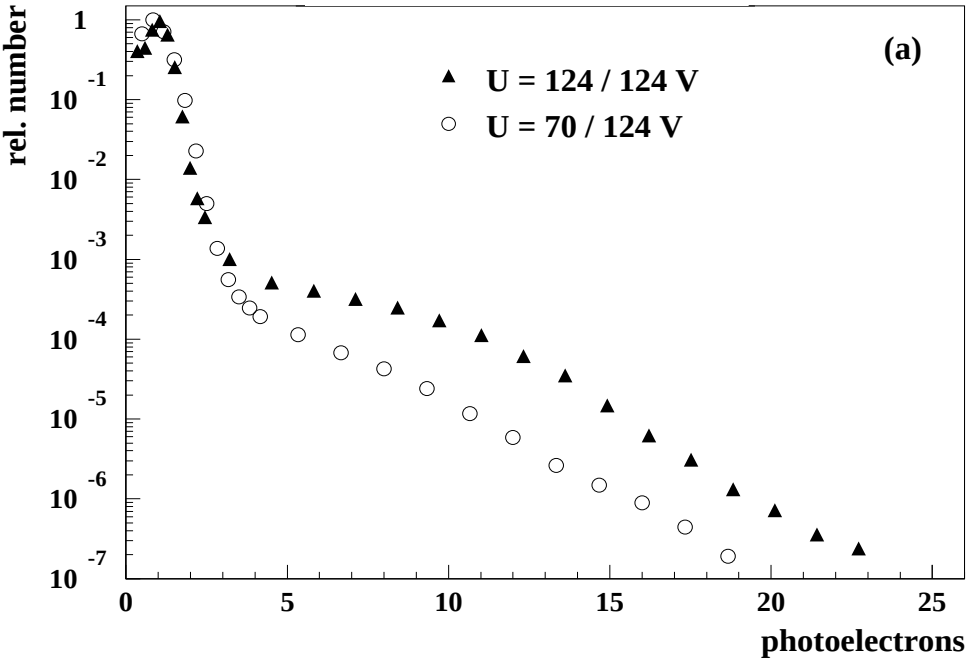
rel. number
1
10^-1
10^-2
10^-3
10^-4
10^-5
10^-6
10^-7
0
5
10
15
20
25
photoelectrons
(a)
U = 124 / 124 V
U = 70 / 124 V

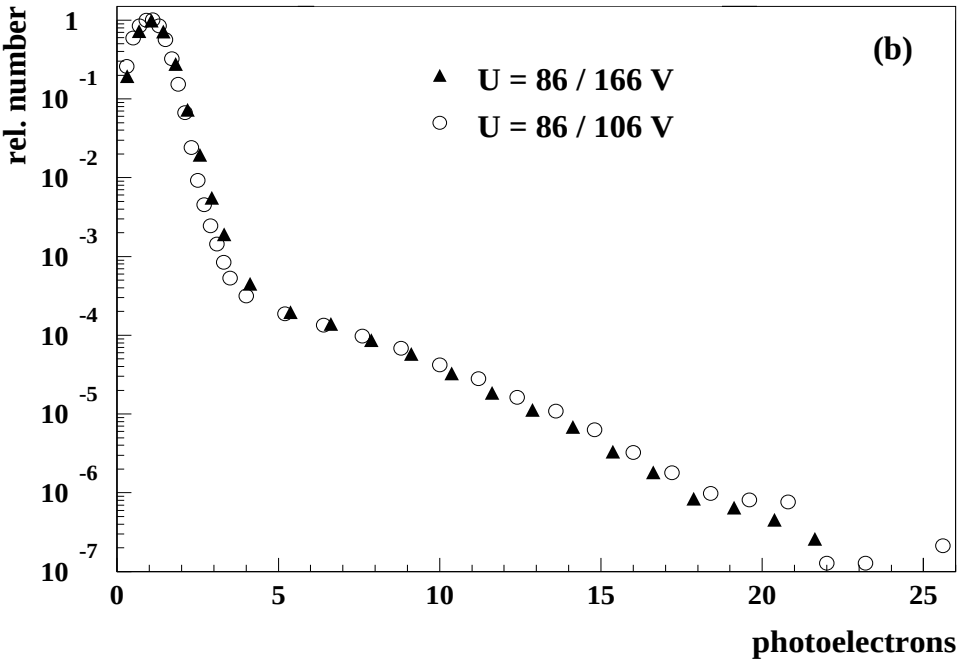
rel. number
1
10^-1
10^-2
10^-3
10^-4
10^-5
10^-6
10^-7
0
5
10
15
20
25
photoelectrons
(b)
U = 86 / 166 V
U = 86 / 106 V

Figure 5: a,b

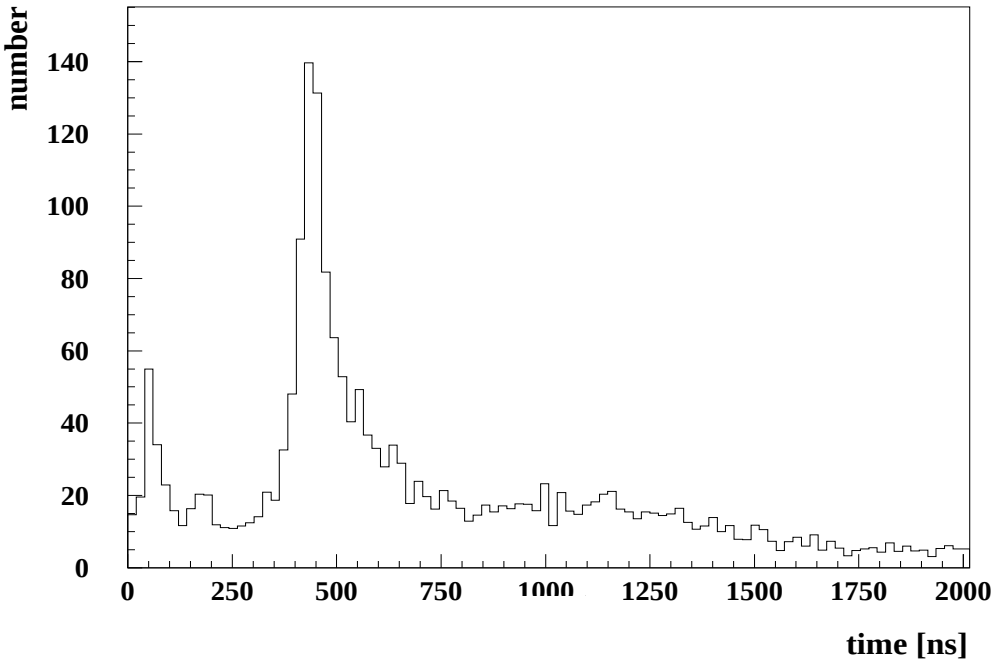
number
140
120
100
80
60
40
20
0
0
250
500
750
1000
1250
1500
1750
2000
time [ns]

Figure 6:

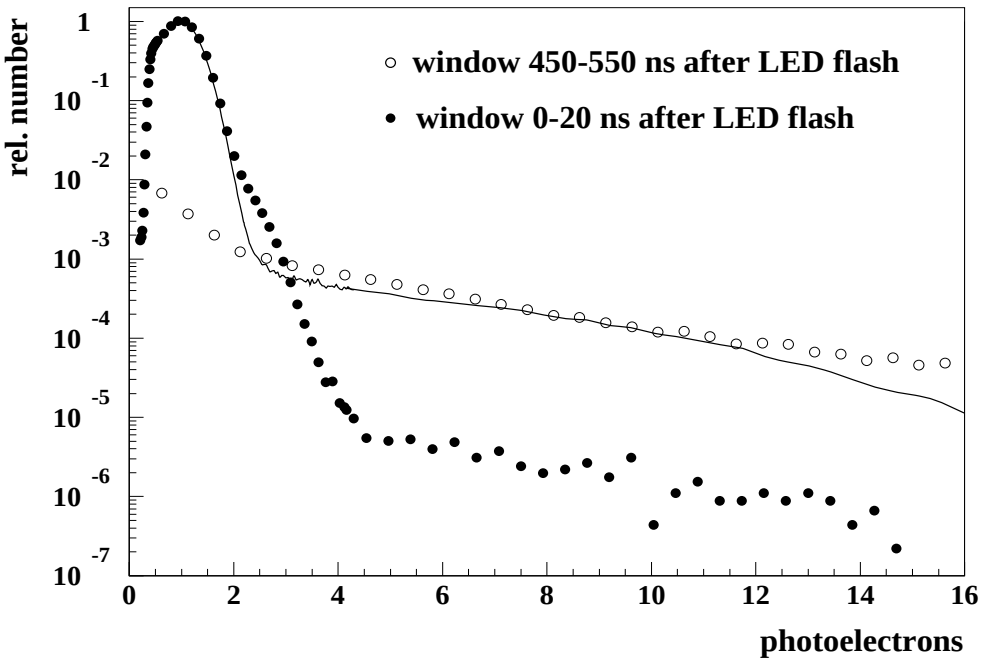
rel. number
1
10^-1
10^-2
10^-3
10^-4
10^-5
10^-6
10^-7
window 450-550 ns after LED flash
window 0-20 ns after LED flash
0
2
4
6
8
10
12
14
16
photoelectrons

Figure 7: